N94- 35638

Comparison of Kalman Filter and Optimal Smoother Estimates of Spacecraft Attitude*

J. Sedlak
Computer Sciences Corporation (CSC)
Lanham-Seabrook, Maryland, USA

Abstract

Given a valid system model and adequate observability, a Kalman filter will converge toward the true system state with error statistics given by the estimated error covariance matrix. The errors generally do not continue to decrease. Rather, a balance is reached between the gain of information from new measurements and the loss of information during propagation. The errors can be further reduced, however, by a second pass through the data with an optimal smoother. This algorithm obtains the optimally weighted average of forward and backward propagating Kalman filters. It roughly halves the error covariance by including future as well as past measurements in each estimate. This paper investigates whether such benefits actually accrue in the application of an optimal smoother to spacecraft attitude determination. Tests are performed both with actual spacecraft data from the Extreme Ultraviolet Explorer (EUVE) and with simulated data for which the true state vector and noise statistics are exactly known.

1. Introduction

Spacecraft attitude determination and sensor calibration are major functions of the Goddard Space Flight Center's (GSFC) Flight Dynamics Facility (FDF). The problem is to extract information about the system state in the presence of perturbing noise. There are a number of ways to attack the problem. These divide broadly into batch and sequential filter methods. While batch methods have been used extensively in the past, sequential filters are also playing an increasingly important role in FDF operations. In particular, real-time extended Kalman filters are currently in use for the Solar, Anomalous, and Magnetospheric Particle Explorer (SAMPEX), the Extreme Ultraviolet Explorer (EUVE) (prototype only), and the soon-to-be-launched next-generation Geostationary Operational Environmental Satellite-I (GOES-I). These are real-time systems designed to solve only for the attitude and the rate bias on each axis.

More elaborate filters are planned for some future missions, such as the X-Ray Timing Explorer (XTE) and the Submillimeter Wave Astronomy Satellite (SWAS). These will include a sequential filter as the central engine of their Attitude Ground Support Systems (AGSS). Various AGSS subsystems are generally responsible for gyro and sensor calibrations. For XTE and SWAS, the gyro calibration will be performed by the AGSS Kalman filter, simultaneously with the attitude. The filter optionally will solve for elements of an expanded state vector, including rate bias, scale factor corrections, and misalignments.

One obvious deficiency of a sequential filter is that only the final state estimate makes use of data throughout the given data span. The XTE and SWAS software will generate improved attitude estimates for an entire data span by using optimal smoothing. A smoother is a sequential method that makes a second pass through the data, so that all the sensor information is available for estimating the state at each time step. Smoothed estimates can be, in effect, weighted averages of forward and backward propagating filters. The uncertainty in the estimate at each step is reduced, compared to the Kalman filter, since it makes use of future as well as past data.

Thus, there are two new aspects to the planned AGSSs: the noise modeling for the expanded state vector in the context of an extended Kalman filter and the smoother algorithm itself. This paper focuses on the smoother algorithm and does not consider the expanded state. The thrust of current investigations is to verify the filter/smoother design, to experiment with tuning parameters, and to examine the improvements in the estimates. It should be stressed that this work is not intended as a definitive statement about the use of smoothing methods for attitude determination. Rather, as just one part

*This work was supported by the National Aeronautics and Space Administration (NASA)/ Goddard Space Flight Center (GSFC), Greenbelt, Maryland, under Contract NAS 5-31500

PRECEDING PAGE BLANK NOT FILMED

of a continuing investigation (see References 1 and 2), it is expected that the smoother results obtained here may be improved in several ways in the future.

The next section presents the extended Kalman filter equations and shows how forward and backward filter results can be combined to form an optimally smoothed estimate. Section 3 discusses some results and comparisons for test cases using EUVE data. The final section gives a summary and conclusions.

2. Theory

As stated above, the smoother can simply form an average of forward and backward filter estimates. What is not obvious is that the optimally smoothed estimate can be written as a linear combination of optimal (i.e., Kalman) filter solutions using only the forward, backward, and smoother error covariance matrices in the weighting coefficients (Reference 3). Conveniently, the smoother error covariance matrix is easily obtainable from the forward and backward filter error covariances.

The starting point for the smoother considered here is the "Unit Vector Filter" (UVF) described in Reference 2. This extended Kalman filter solves for attitude and gyro bias using a particularly simple observation noise model. Onboard measurements of Sun and star unit vectors are assumed to be perturbed by random noise uniformly on all three axes; hence, the sensor noise covariance matrix is a constant times the identity matrix.

For both the UVF and the smoother described below, a distinction must be made between the full 7-component state vector, comprised of the attitude quaternion and the gyro bias vector, and the 6-component error state (Reference 4). The small-angle rotation from the true to the estimated attitude can be written as a 3-component error vector, one dimension less than the 4-component quaternion needed for an unambiguous representation of the attitude in inertial space.

Thus, in outline, the UVF proceeds as follows for either forward or backward processing: The full state vector and the 6x6-dimensional state error covariance matrix are propagated from the current time to the next sensor measurement. A prediction vector, based on the estimated attitude and a reference vector, is subtracted from the observation to obtain a residual vector. The residual, weighted by the Kalman gain matrix, yields the new estimated error state. The propagated quaternion is rotated by the estimated attitude error, and the gyro bias is corrected by the bias error. The error state then is discarded since its information has been incorporated into the full state. Finally, the Kalman gain also is used to update the state error covariance matrix.

Kalman Filter

The state evolution can be integrated over a time step Δt to obtain discrete-step propagation equations. Derivations can be found in Reference 5 and in those previously cited. For the backward filter, the index k increases as the time t_k decreases. The attitude quaternion is propagated as

$$q_{k|k-1} = \left\{ \cos\left(\frac{\theta}{2}\right) I_4 + \frac{1}{\omega_{k|k-1}} \sin\left(\frac{\theta}{2}\right) \Omega(\vec{\omega}_{k|k-1}) \right\} q_{k-1|k-1} \tag{1}$$

where the time interval is $\Delta t = t_k - t_{k-1}$, and

$$\theta \equiv \omega_{k|k-1} \Delta t \tag{2}$$

The $k|j$ notation indicates a quantity estimated using sensor data through time t_j, and propagated (if $k \neq j$) to time t_k.

Equation (1) is approximate in that it assumes the angular rate is constant over Δt. The estimated rate for this interval is the gyro output $\vec{u}_k$, corrected with the latest bias estimate:

$$\vec{\omega}_{k|k-1} = \vec{u}_k - \vec{b}_{k|k-1} \tag{3}$$

In many cases, $\vec{u}_k$ is an average for the time interval, generated by a rate integrating gyro unit.

The matrix Ω is

$$\Omega(\vec{\omega}) = \begin{bmatrix} 0 & \omega_z & -\omega_y & \omega_x \\ -\omega_z & 0 & \omega_x & \omega_y \\ \omega_y & -\omega_x & 0 & \omega_z \\ -\omega_x & -\omega_y & -\omega_z & 0 \end{bmatrix} \tag{4}$$

The estimated gyro bias propagates as a constant:

$$\vec{b}_{k|k-1} = \vec{b}_{k-1|k-1} \tag{5}$$

The error state is

$$x_k = \begin{bmatrix} \vec{\alpha}_k \\ \Delta\vec{b}_k \end{bmatrix} \tag{6}$$

where the true (but unknown) error rotation vector $\vec{\alpha}$ is related to the true and estimated quaternions by

$$q_k = \delta q_k^{-1} \otimes q_{k|k-1} \tag{7}$$

with

$$\delta q_k^{-1} \approx \begin{bmatrix} -\vec{\alpha}_k/2 \\ 1 \end{bmatrix} \tag{8}$$

The product in Equation (7) is defined so as to combine quaternions in the same order as attitude matrices. Also, the inverse quaternion is used in Equation (7) to simplify signs elsewhere. For brevity, only the first order approximation is shown in Equation (8) and elsewhere for the error quaternion. In practice, one must either add a normalization step or use the full trigonometric relationship in Equation (8).

Similarly, the true gyro bias, its estimate, and the unknown correction are related additively:

$$\vec{b}_k = \vec{b}_{k|k-1} + \Delta\vec{b}_k \tag{9}$$

Although dynamics noise does not affect the mean propagation of the full state described above, it is needed for the error covariance propagation. Perturbations are assumed to enter the problem as zero-mean white noise in the true angular rate

$$\vec{\omega} = \vec{u} - \vec{b} - \vec{\eta}_1 \tag{10}$$

and in the true gyro bias evolution

$$\frac{d\vec{b}}{dt} = \vec{\eta}_2 \tag{11}$$

From these, one can form a 6-component noise vector $\eta^T \equiv [\vec{\eta}_1^T, \vec{\eta}_2^T]$. Its 2-time expectation is

$$E[\eta(t)\eta^T(t')] = Q(t)\delta(t-t') \tag{12}$$

The matrix $Q(t)$ is the spectral density

$$Q(t) = \begin{bmatrix} \sigma_1^2 I_3 & 0 \\ 0 & \sigma_2^2 I_3 \end{bmatrix} \tag{13}$$

where I_3 is the 3×3 identity matrix, and σ_1^2, σ_2^2 model the gyro drift rate noise and drift rate ramp noise, respectively. From this noise model, one can show that the state error covariance

$$P_{k|j} = E[x_{k|j}\, x_{k|j}^T] \tag{14}$$

propagates according to

$$P_{k|k-1} = \Phi P_{k-1|k-1} \Phi^T \pm Q_k \tag{15}$$

where the plus sign is used when $\Delta t > 0$ and the minus sign when $\Delta t < 0$. The propagation matrix is

$$\Phi = \begin{bmatrix} \phi & \psi \\ 0_{3\times3} & I_3 \end{bmatrix} \tag{16}$$

where the submatrices are

$$\phi = I_3 - \sin\theta \frac{[\vec{\omega}\times]}{\omega} + (1-\cos\theta)\frac{[\vec{\omega}\times]^2}{\omega^2} \tag{17}$$

and its integral

$$\psi = I_3 \Delta t + (\cos\theta - 1)\frac{[\vec{\omega}\times]}{\omega^2} + (\theta - \sin\theta)\frac{[\vec{\omega}\times]^2}{\omega^3} \tag{18}$$

The antisymmetric cross-product matrix is denoted

$$[\vec{\omega}\times] \equiv \begin{bmatrix} 0 & -\omega_z & \omega_y \\ \omega_z & 0 & -\omega_x \\ -\omega_y & \omega_x & 0 \end{bmatrix} \tag{19}$$

The process noise matrix is

$$Q_k = \begin{bmatrix} C & \sigma_2^2 \chi \\ \sigma_2^2 \chi^T & \sigma_2^2 \Delta t \end{bmatrix} \tag{20}$$

where the matrix χ is the integral of ψ

$$\chi = I_3 \frac{\Delta t^2}{2} + (\sin\theta - \theta)\frac{[\vec{\omega}\times]}{\omega^3} + \left(\cos\theta - 1 + \frac{\theta^2}{2}\right)\frac{[\vec{\omega}\times]^2}{\omega^4} \tag{21}$$

and C is the integral of a constant plus $\psi\psi^T$

$$C = \sigma_1^2 I_3 \Delta t + \sigma_2^2\left[\frac{I_3 \Delta t^3}{3} + 2\frac{[\vec{\omega}\times]^2}{\omega^5}\left(\sin\theta - \theta + \frac{\theta^3}{6}\right)\right] \tag{22}$$

The update step uses the standard Kalman filter equations (Reference 5):

$$x_{k|k} = K_k \vec{y}_k \tag{23}$$

where the a priori state is zero since x is an error state. The residual $\vec{y}_k$ is discussed below. The Joseph-stabilized error covariance update is

$$P_{k|k} = (I_3 - K_k H_k) P_{k|k-1} (I_3 - K_k H_k)^T + K_k R_k K_k^T \tag{24}$$

The Kalman gain matrix is

$$K_k = P_{k|k-1} H_k^T \left[H_k P_{k|k-1} H_k^T + R_k\right]^{-1} \tag{25}$$

and the UVF observation model assumes the sensor noise covariance matrix to be

$$R_k = \sigma_k^2 I_3 \tag{26}$$

where σ_k here is the noise standard deviation on each component of the unit vector.

The residual

$$\vec{y}_k = \hat{w}_k - \hat{w}_{k|k-1} \tag{27}$$

is the difference between the observed unit vector and the prediction

$$\hat{w}_{k|k-1} = A_{k|k-1} \hat{v}_k \tag{28}$$

where A is the attitude matrix and $\hat{v}_k$ is the reference vector. Model the actual observation as

$$\hat{w}_k = \frac{A_k \hat{v}_k + \vec{n}_k}{|A_k \hat{v}_k + \vec{n}_k|} \tag{29}$$

where $\vec{n}_k$ is a Gaussian distributed white noise sequence of strength σ_k on each axis. References 2 and 6 show that one can safely neglect the difference between the covariance of the sensor noise implied by Equation (29) and that given in Equation (26). (This freedom arises because the filter is totally insensitive to the noise component along the observed vector.)

The observation sensitivity matrix is the partial of the observation vector with respect to the error state vector, evaluated at the current estimate. Analogous to Equation (7), the true attitude matrix is related to its estimate by the small-angle rotation, $-\vec{\alpha}_k$. Representing the rotation as a matrix exponential, one has

$$\begin{aligned} A_k \hat{v}_k &= \exp([\vec{\alpha}_k \times]) A_{k|k-1} \hat{v}_k \\ &\approx (I + [\vec{\alpha}_k \times]) \hat{w}_{k|k-1} \\ &= \hat{w}_{k|k-1} - [\hat{w}_{k|k-1} \times] \vec{\alpha}_k \end{aligned} \tag{30}$$

where the sign flip occurs when $\hat{w}$ and $\vec{\alpha}$ are interchanged through the cross product. Inserting this into Equation (29) and expanding, one finds the sensitivity matrix is

$$H_k = \left(-[\hat{w}_{k|k-1} \times] \ \vdots \ 0_{3\times3} \right) \tag{31}$$

The zero submatrix appears because the observation is independent of the gyro bias part of the error state.

Optimal Smoother

As the forward filter proceeds, the a posteriori (post-update) full state and error covariance are periodically saved. Observation data and reference vectors are also saved so that star identification and data adjustment need not be repeated. To run the backward Kalman filter, the saved values are read and processed in reverse order. The only difference from the forward filter is that the sign of the process noise must be flipped for the covariance propagation, as indicated in Equation (15). This ensures that the uncertainty in the estimate grows whichever way one propagates.

The smoother runs simultaneously with the backward filter. The backward state estimate is propagated to the time of a saved forward solution. If this is also a measurement time, the state vectors are combined prior to updating the backward estimate (the information from that measurement having already been used in the forward filter).

One complication is that the smoother cannot combine the state vectors directly. The 6×6- covariance matrices apply to the rotation vector and bias correction, not to the full state. It is necessary to express the smoother algorithm also in terms of a small-angle rotation. Were it not for this complication, one would simply form the smoother covariance

$$P_k^s = \left(P_{k|k}^{f\ -1} + P_{k|k-1}^{b\ -1} \right)^{-1} \tag{32}$$

and obtain the smoothed state (generically referred to as X here) as the weighted average:

$$X_k^s = P_k^s \left(P_{k|k}^{f\ -1} X_{k|k}^f + P_{k|k-1}^{b\ -1} X_{k|k-1}^b \right) \tag{33}$$

The f, b, s notation refers to forward, backward, and smoothed values, and some care must be taken in interpreting the $k\,|\,k-1$ subscript on the backward estimates (the indices refer to the update sequence, not the time sequence). Rearranging Equation (32) yields

$$P_k^s P_{k|k}^{f\ -1} = I - P_k^s P_{k|k-1}^{b\ -1} \tag{34}$$

hence

$$X_k^s = X_{k|k}^f + P_k^s P_{k|k-1}^{b\ -1} \left(X_{k|k-1}^b - X_{k|k}^f \right) \tag{35}$$

Thus, the smoothed state is the forward state plus a correction proportional to the difference between the states.

Analogously, one can use the small-angle rotation between the attitudes and the gyro bias difference to correct the forward state. Noting that it is $-\vec{\alpha}$ in Equations (7) and (8) that rotates from the estimated to the true state, one defines Δq and $\Delta\vec{\alpha}$ by

$$\Delta q = \left(q^b \otimes q^{f*}\right)^* = q^f \otimes q^{b*} \tag{36}$$

and

$$\Delta q \approx \begin{bmatrix} \Delta\vec{\alpha}/2 \\ 1 \end{bmatrix} \tag{37}$$

The sequence indices have been suppressed in these and the following equations. So, $-\Delta\vec{\alpha}$ rotates from the forward to the backward attitude estimate. Similarly, $\Delta\vec{b}$ is the difference from the forward to the backward bias estimate

$$\Delta\vec{b} = \vec{b}^b - \vec{b}^f \tag{38}$$

This is then weighted using the covariances

$$\begin{bmatrix} \delta\vec{\alpha} \\ \delta\vec{b} \end{bmatrix} = P^s P^{b^{-1}} \begin{bmatrix} \Delta\vec{\alpha} \\ \Delta\vec{b} \end{bmatrix} \tag{39}$$

Finally, these are combined with the forward estimate, as in Equation (35), to obtain the smoothed state

$$q^s \approx \begin{bmatrix} -\delta\vec{\alpha}/2 \\ 1 \end{bmatrix} \otimes q^f \tag{40}$$

and

$$\vec{b}^s = \vec{b}^f + \delta\vec{b} \tag{41}$$

One can see how the smoother works most easily by inspecting Equations (32) and (33). If one of the forward or backward error covariances is much larger than the other, then its inverse contributes little to the sum in Equation (32). In that case the smoother error covariance approximately equals the smaller of P^f and P^b. In Equation (33), the inverse of the large covariance suppresses the contribution from that state, and P^s times the inverse of the other covariance is close to the identity. Thus, the smoothed state closely equals the state with the smaller covariance. Alternatively, when P^f and P^b are similar, the inverse of the sum in Equation (32) yields a smoother covariance half as large, and the smoothed state is roughly the average of the forward and backward states.

The forward filter starts with a relatively large uncertainty, thus the smoothed state should be dominated by the backward estimate until observation data bring the forward covariance down. Similarly, the backward state is initialized with a very large covariance, so the smoothed state should nearly equal the forward solution near the end of the data span.

3. Results

This section presents results from two sets of tests run on the first version of the optimal smoother. The first tests make use of actual flight data from the EUVE spacecraft. These data span two orbits on December 16, 1992, when EUVE was in Survey mode. In this mode, the spacecraft has its body x-axis (the roll axis) pointed away from the Sun, and it maintains a steady 3-revolution-per-orbit (3-rpo) roll rate. It remains nearly stationary about its y- and z-axes (pitch and yaw).

The only measurements used in these tests are from two fixed-head star trackers (FHSTs) and the rate-integrating gyros. When not in Earth shadow, the Sun vector is used to help identify stars by a dot product test, but it is not included in

the filter update. The FHST 1σ noise parameters are set to 0.01 deg, due mainly to the time tag uncertainty times the roll rate. The gyro noise parameters are taken to be $\sigma_1^2 = 10^{-13}$ **rad**^{2}/**sec** and $\sigma_2^2 = 10^{-19}$ **rad**^{2}/**sec**^{3}.

Figure 1 shows the forward filter solutions for the pitch and yaw axes as solid lines. The roll angle varies from 0 to 360 deg six times during this period and is not shown. These are similar to results presented in Reference 2, except for some significant improvements in the gyro processing in the current version. For comparison, the solutions generated by the onboard computer (OBC) filter are shown as dashed lines. These two filters are fairly similar in design. The steps in the yaw angle near $t =$ 5000 sec and 11000 sec are small maneuvers performed each orbit to keep the roll axis pointing away from the Sun. At the same time, there is a roll adjustment to maintain the roll phase relative to the orbital position.

The sensor update history is shown in Figure 2. The points indicate the times of occurrence of filter updates for the two star trackers. The gaps in the update history appear when the trackers are facing the Earth.

The small-angle deviations between the OBC and the forward filter solutions are presented in Figure 3. On this scale, initial transients and the jitter due to gyro noise are more apparent. The backward filter results look quite similar, except that the "initial" transients occur at the end of the data span. The relatively large deviations in roll angle at the times of the roll phase adjustment are errors in the OBC solution, probably caused by its gyro smoothing algorithm. The 3-rpo oscillation derives from a small difference between the UVF and OBC estimated Euler axes, which leads to body frame errors being modulated at the rotation rate.

Figure 4 shows the smoother attitude estimates in the same format as Figure 3. It is clear that the smoother has had only a small effect on the solutions. Some apparent improvement is visible near $t =$ 3000 sec (where a gyro counter rollover occurs) and the forward and backward transients are completely removed.

Gyro biases shown in Figure 5 are in excellent agreement with OBC-determined biases (not shown) and with those obtained from the ground support system for a similar time span (dashed lines). The offset of roughly 0.01 deg/hr is comparable to the 1σ uncertainty in the AGSS estimate (Reference 7). Forward, backward, and smoothed solutions are shown for the body frame z-axis gyro drift rate. Solutions are similar for the x- and y-axes. The transients apparent in the forward and backward estimates are completely removed in the smoothed bias. There also is a visible reduction in noise.

One internal figure of merit for the filter and smoother is the error covariance. Uncertainties for the attitude and bias are obtained separately as the square root of the sum of the first three and the last three elements of the covariance matrix. Figure 6 overlays these uncertainties for the forward, backward, and smoothed solutions. Several features are apparent: the smoother errors equal the forward errors at the end of the time span, and equal the backward errors at the beginning, as expected from Equation (32). The errors grow due to process noise during the data gaps between star observations. The Kalman filter errors are lowest at the beginning or ending times, after each has had access to all of the data. The smoother always has access to the entire data span, but its errors are lowest near the middle since that point is closest in time to all the data, on average. This minimizes the contribution from the process noise.

A second internal check is to obtain the mean gyro bias and the root-mean-square (RMS) deviation from the mean. This is useful since the bias is expected to be very nearly constant. As Figure 5 shows, the deviations are very small. Statistics are gathered from the second orbit for the forward filter, the first orbit for the backward filter, and from the middle for the smoother. The three-axis root-sum-square averages of these orbit-averaged RMS deviations are 0.0026 deg/hr for both the forward and backward filters, and 0.0011 deg/hr for the smoother, somewhat smaller than the uncertainties deduced from the covariances shown in Figure 6. The filter/smoother covariance ratio is close to 2, as expected (see Equation (32) and the discussion at the end of Section 2).

A similar statistical check of the attitude is not useful because there is no available truth model. The deviations in Figure 3 are caused equally by errors in the UVF and the OBC filters. The OBC errors mask any improvements due to the smoother. For this reason, the smoother was tested using a simulated data set for which the true state is known. The true rates are taken to be (3 rpo, 0, 0), but the gyro output is perturbed by white noise and a randomly walking gyro bias as in Equation (10). The noise on the simulated star observations is Gaussian distributed, with width σ = 0.01 **deg**. The resulting deviations with the truth model are shown in Figure 7. In this case, the uncertainty (as defined for Figure 6) and the deviation from the truth model are in fairly close agreement. When averaged over an orbit, and averaging the

three axes, the forward and backward filters both have uncertainties of 3.8 arc sec, and RMS deviations of 3 to 4 arc sec. The smoother uncertainty is 2.4 arc sec and RMS deviation is 2.1 arc sec.

4. Conclusions

An optimal smoother for estimating spacecraft attitude and gyro bias has been developed and tested using both EUVE flight data and simulated data. It has been shown that the algorithm converges and yields reasonable results. The solutions have been tested for internal consistency by examining the error covariances and the RMS variations of those parameters that are expected to be constant (the gyro biases). In addition, the smoother was tested using a simple simulation. The tuning parameters then could be chosen exactly to match the model, and the resulting error covariances were found to match the actual solution statistics.

Continuing investigations may go in two different directions. The expanded state vector to be used by some future missions for full gyro calibrations should be tested for convergence under varying observability conditions. Designs for those filter/smoothers also include a more general process noise matrix that allows for a different noise parameter on each axis. This should be tested for its ability to obtain good attitudes in the presence of gyro degradation on selected axes.

Another direction for future studies is to look at alternative smoother algorithms. There are a few different ways to re-express the simple forward/backward average implemented here. There are expected advantages to these other methods in terms of central processing unit (CPU)-time efficiency. There also is a theoretical difference that may be significant. The current smoother uses the final forward state estimate as the initial value for the backward filter. This imposes strong correlations between the forward and backward states that should not be there. To cure this, the backward error covariance is taken to be the forward covariance times a large factor (typically 10^{12} in the test cases). It is expected that this large covariance forces the backward filter to put full confidence in the sensor data, and almost instantly forget its initial value. However, there may be correlations that persist and leave the smoother state suboptimal. The problem can be avoided by redefining the backward filter in terms of $\boldsymbol{P}^{-1}$ and a new state variable, $\boldsymbol{P}^{-1}\boldsymbol{x}$. Initializing these to zero implies zero a priori information and no correlation with the forward filter.

References

1. M. Challa, et al., "Real-Time Attitude Determination and Gyro Calibration," in *Proceedings, Flight Mechanics/Estimation Theory Symposium*, NASA Goddard Space Flight Center, May 1991

2. J. Sedlak and D. Chu, "Kalman Filter Estimation of Attitude and Gyro Bias With the QUEST Observation Model," in *Proceedings, AAS/GSFC International Symposium on Space Flight Dynamics*, April 1993

3. D. C. Fraser and J. E. Potter, "The Optimum Linear Smoother as a Combination of Two Optimum Linear Filters," *IEEE Trans. on Automatic Control*, Vol. 7, No. 8, August 1969

4. E. J. Lefferts, F. L. Markley, and M. D. Shuster, "Kalman Filtering for Spacecraft Attitude Estimation," *J. Guidance, Control, and Dynamics*, Vol. 5, No. 5, Sept.–Oct. 1982

5. A. Gelb, ed., *Applied Optimal Estimation*, Cambridge: MIT Press, 1974

6. M. D. Shuster, "Kalman Filtering of Spacecraft Attitude and the QUEST Model," *J. Astronaut. Sci.*, Vol. 38, No. 3, July–Sept. 1990

7. W. Davis, et al., "Postlaunch Calibration of Spacecraft Attitude Instruments," in *Proceedings, AAS/GSFC International Symposium on Space Flight Dynamics*, April 1993

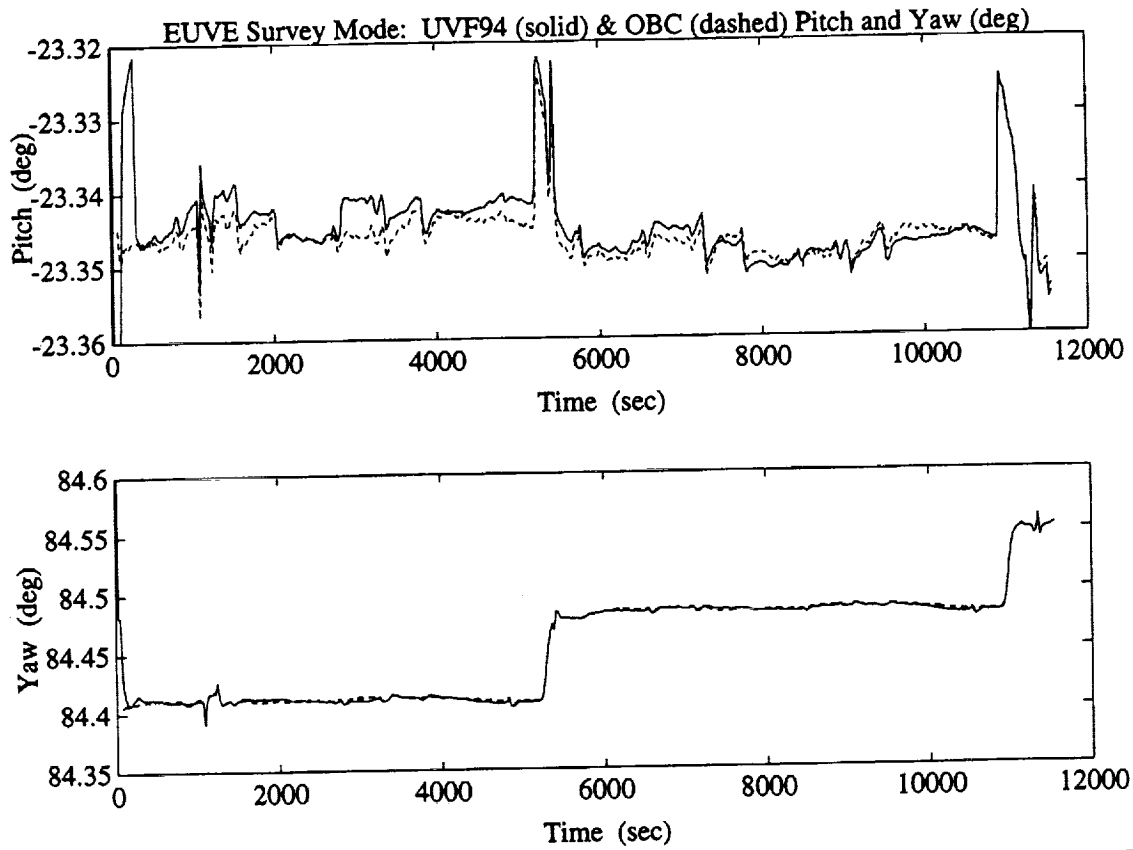

Figure 1. Forward Filter (solid lines) and OBC (dashed lines) Estimates of Pitch and Yaw Angles Versus Time

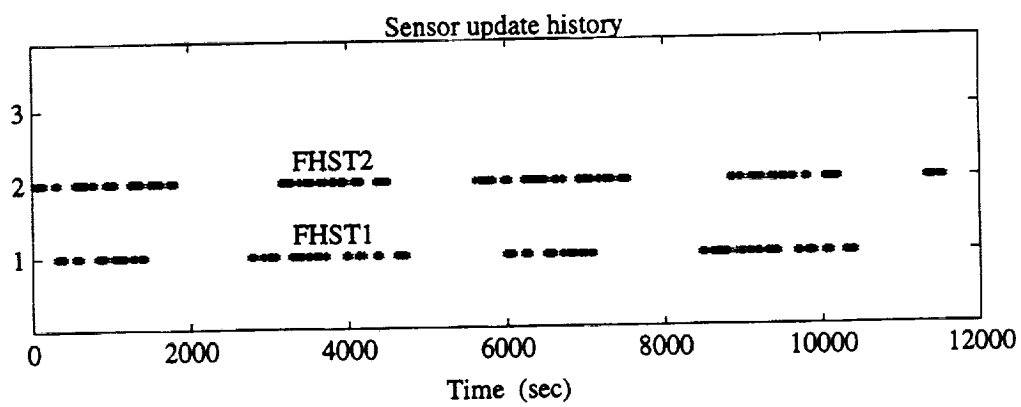

Figure 2. Sensor Update History

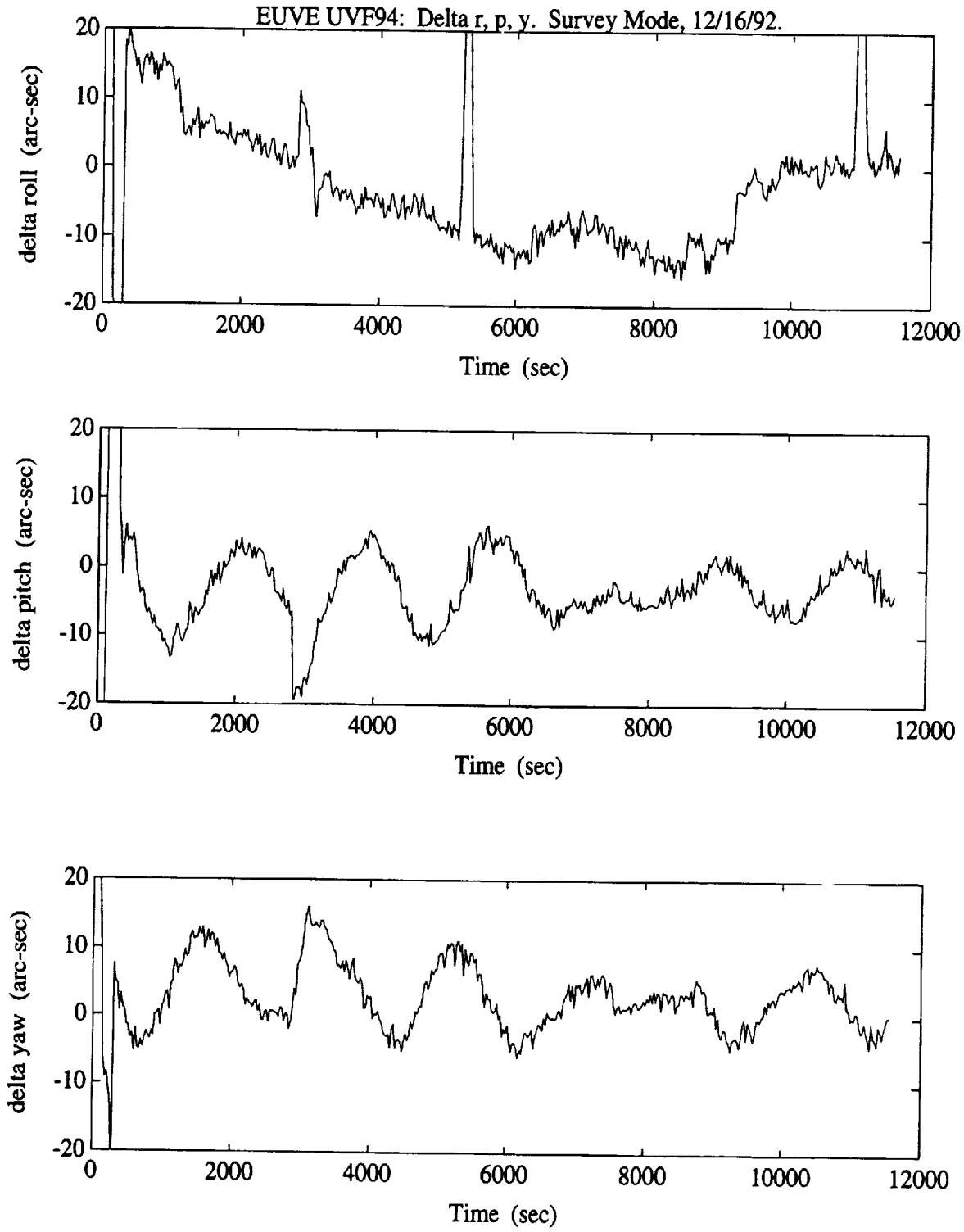

Figure 3. Delta Roll, Pitch, and Yaw Versus Time From Comparison of EUVE Forward Filter and OBC Quaternion Estimates

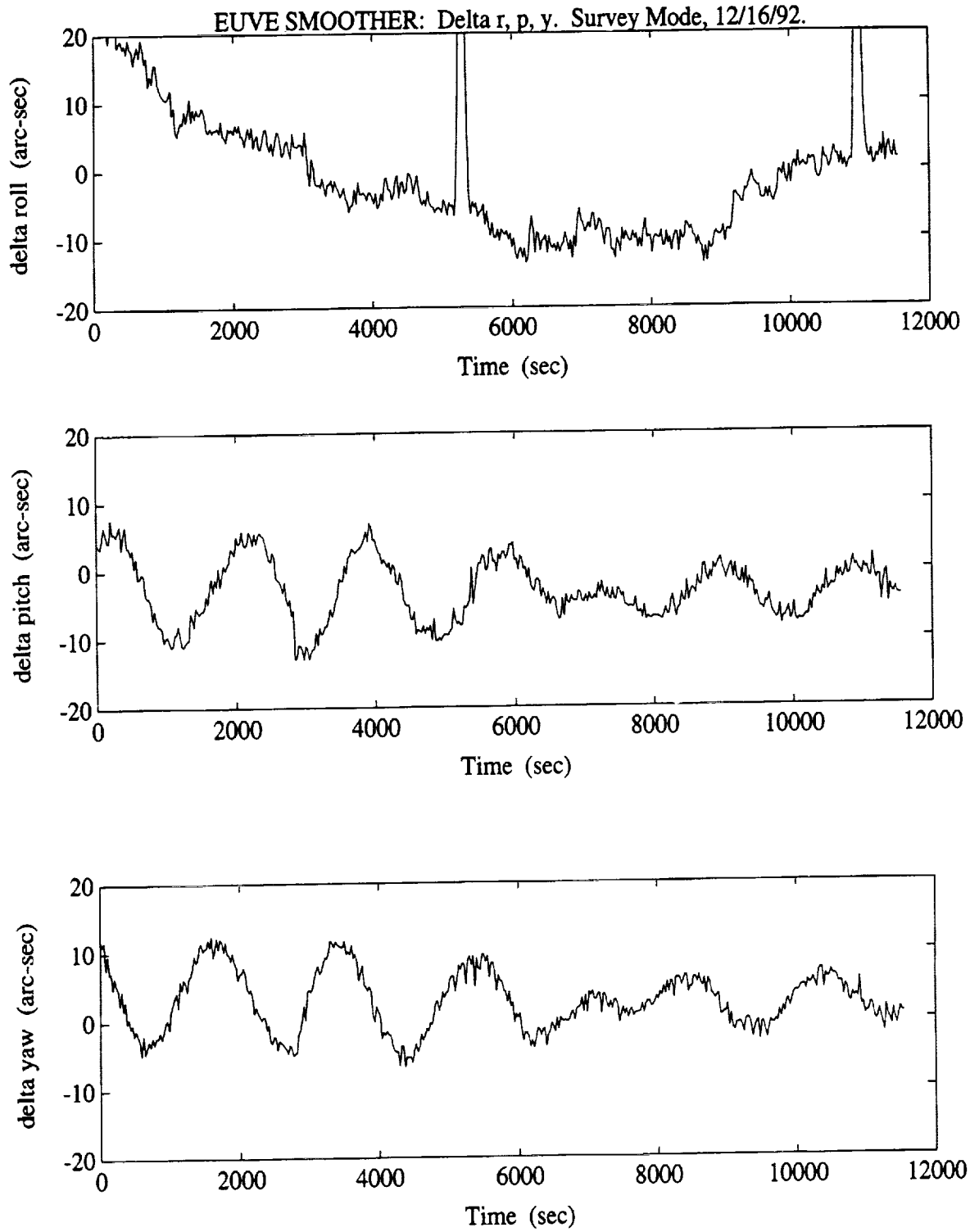

Figure 4. Delta Roll, Pitch, and Yaw Versus Time From Comparison of EUVE Optimal Smoother and OBC Quaternion Estimates

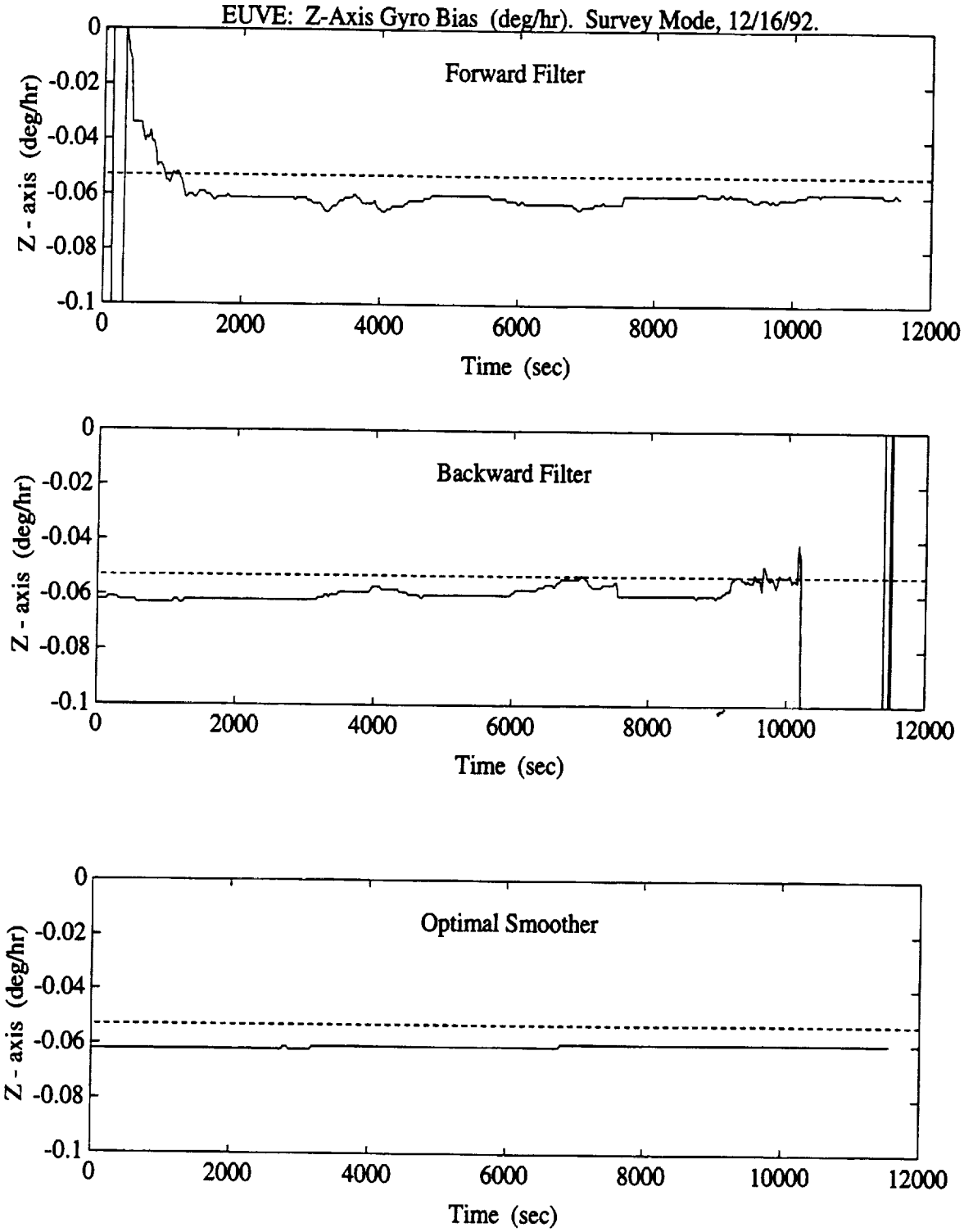

Figure 5. Forward Filter, Backward Filter, and Optimal Smoother Estimates of Body Z-Axis Gyro Drift Bias Versus Time (dashed lines indicate AGSS estimate)

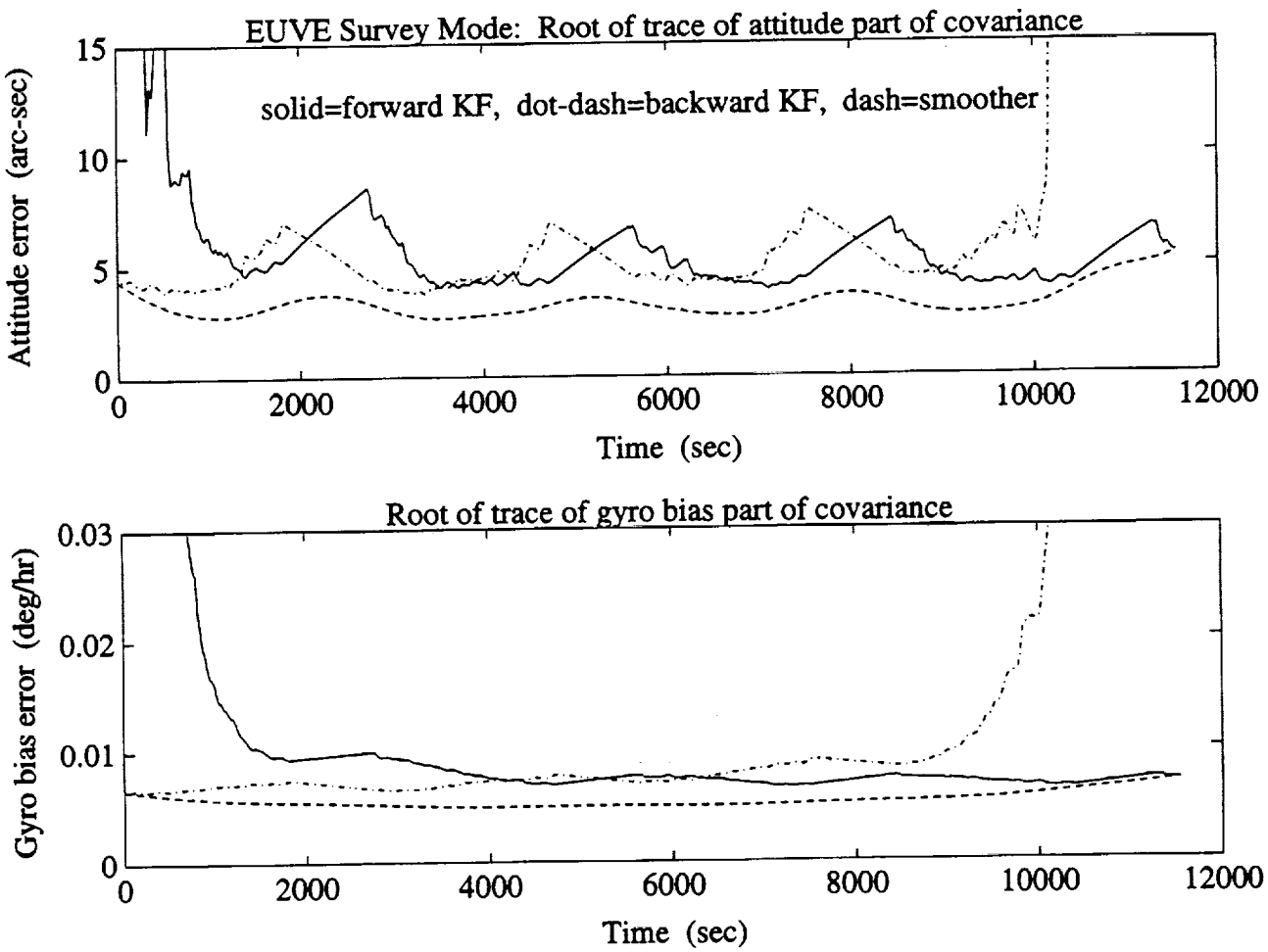

Figure 6. Forward (solid), Backward (dot-dash), and Smoother (dashed) Attitude and Gyro Bias Uncertainties Versus Time

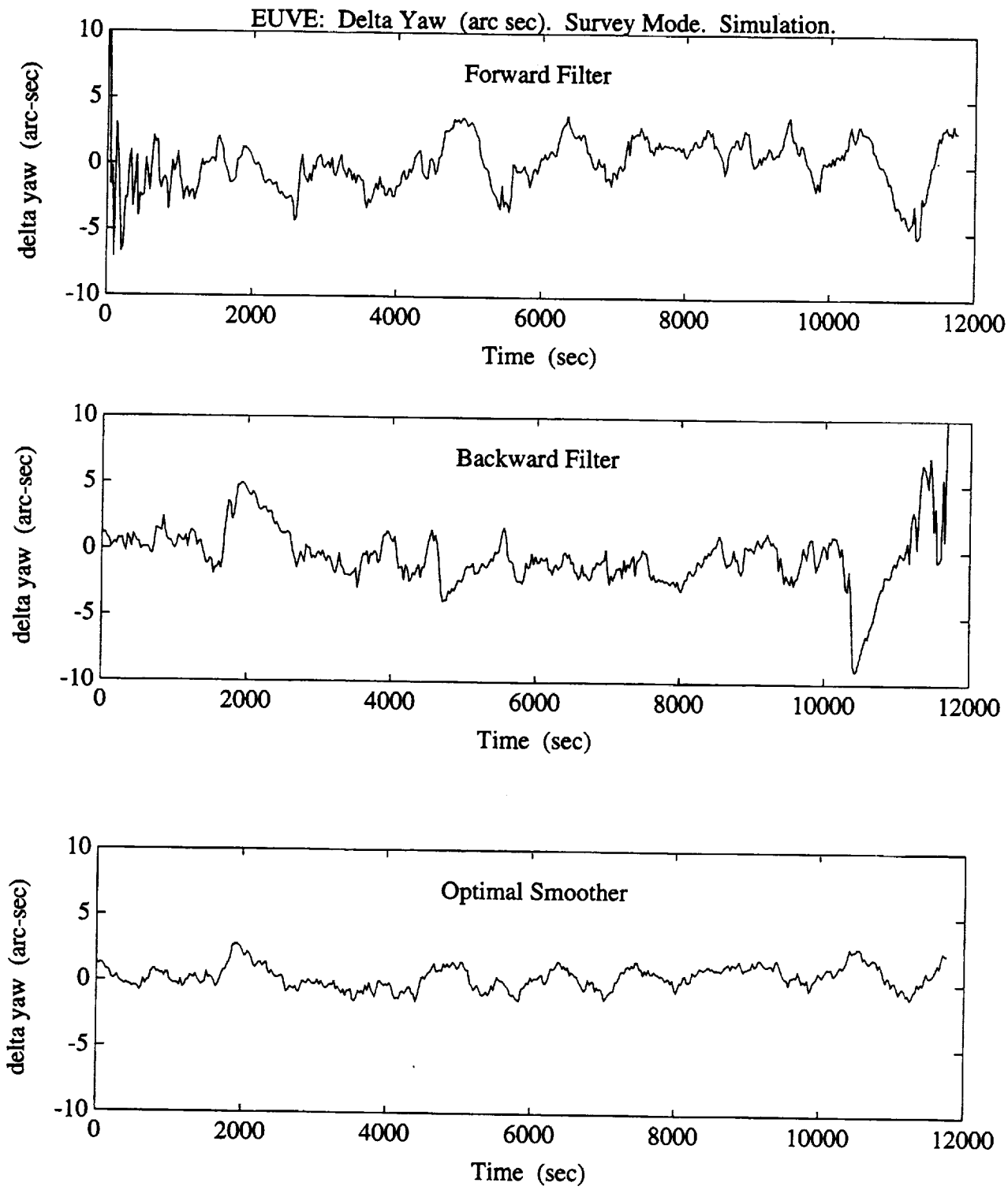

Figure 7. Delta Yaw Versus Time From Comparison of Estimates and Simulation Truth Model